Rapid Communications

Role of nuclear symmetry in below-threshold harmonic generation of molecules

Peng-Cheng Li,[1,2,*] Yae-Lin Sheu,[3,4] and Shih-I Chu[4,5,†]

[1]*Research Center for Advanced Optics and Photoelectronics, Department of Physics, College of Science, Shantou University, Shantou, Guangdong 515063, China*

[2]*Key Laboratory of Intelligent Manufacturing Technology of MOE, Shantou University, Shantou, Guangdong 515063, China*

[3]*Department of Statistics, University of Washington, Seattle, Washington 98195, USA*

[4]*Center for Quantum Science and Engineering, Department of Physics, National Taiwan University, Taipei 10617, Taiwan*

[5]*Department of Chemistry, University of Kansas, Lawrence, Kansas 66045, USA*

(Received 26 September 2019; published 7 January 2020)

Below-threshold harmonic generation (BTHG) is one of few potential methods for the generation of novel vacuum-ultraviolet (VUV) light sources. However, most previous studies have focused on the atomic BTHG; a comprehensive understanding of the molecular BTHG is valuable for the advancement of this field. Here, we present an *ab initio* study of the role of nuclear symmetry on BTHG of both homonuclear and heteronuclear diatomic molecules. We reveal very distinctive electronic dynamical behaviors in molecular BTHG by identifying subtle multiple-channel contributions. In particular, it is found that the channels associated with the electron-nuclear coupling from light nuclear core to heavy nuclear core of the asymmetric molecules play an important role in the constructive interference of the harmonic emission, leading to a significant enhancement of the BTHG. Our results suggest that asymmetric molecular systems can be used for substantial improvement of the molecular BTHG-based VUV light sources.

DOI: 10.1103/PhysRevA.101.011401

High-order harmonic generation (HHG) has been one of the most significant and extensively studied strong-field processes in the last decade. It can lead to fruitful applications in ultrafast processes and transient spectroscopy in atomic, molecular, and condensed matter systems, as well as in chemical reactions, etc. [1–3]. The HHG spectrum above the ionization threshold is well understood by a semiclassical three-step model [4,5]. First, the bound electron is freed by tunneling ionization and then accelerated in an applied laser field. Last, the electron can be driven back toward the parent ion to recombine with the ground state and generates the harmonics. The HHG spectrum is characterized by a rapid drop at low orders followed by a broad plateau where all the harmonics have the similar amplitude and finally a sharp cutoff beyond which no further harmonic emission is observed.

In the past, most studies have focused on the HHG above the ionization threshold. Recently the HHG below the ionization threshold has become a subject of immense interest. It has been shown that below-threshold harmonic emission can provide a potential way to produce novel strong light sources [6,7] in the vacuum-ultraviolet band due to high conversion efficiency. Although considerable attention has been paid to the exploration of the dynamical origin of the below-threshold harmonic generation (BTHG) [8,9], most recent studies so far have only focused on the atomic BTHG. The molecular BTHG becomes much more complex due to the presence of extra internuclear degrees of freedom. There are two challenges for the exploration of the dynamical origin of the molecular BTHG. First, the *ab initio* treatment of the molecular BTHG can be very difficult for complicated physical processes. Second, an accurate analysis of the spectral and temporal structure of the BTHG using the traditional time-frequency analysis methods, such as widely used wavelet and Gabor transform [10,11], is generally not possible because their time-frequency spectra of the BTHG contain many obscure features [12] in contrast to the usually clean ones seen in many previous studies of the molecular HHG on above- and near-threshold regimes [13–17]. More recently, spectral characteristics of the BTHG of H_2^+ molecular ions either in linearly or nonlinearly polarized laser fields have been studied [18,19]. However, how the nuclear symmetry influences the channel selection and the conversion efficiency in the molecular BTHG remains still largely unexplored.

In this work, we explore the dynamical role of the nuclear symmetry on the molecular BTHG by studying homonuclear and heteronuclear diatomic molecular systems in an intense infrared laser field. We perform fully *ab initio* and accurate numerical solution of the three-dimensional time-dependent Schrödinger equation (TDSE) [20] for one-electron diatomic molecular systems and extend the self-interaction-free time-dependent density functional theory (TDDFT) [21–24] for the accurate treatment of multielectron diatomic molecular systems. Both the TDSE and TDDFT can be accurately and efficiently solved by means of the time-dependent generalized pseudospectral method (TDGPS) [25] in the prolate spheroidal coordinates. Once the time-dependent wave function is available, we can calculate the HHG power spectrum by Fourier transformation of time-dependent dipole moment. Combining the spectral and temporal spectra determined from the synchrosqueezed transform (SST) [26] recently developed and the dynamical channel information obtained by solving

*Corresponding author: pchli@stu.edu.cn
†Corresponding author: sichu@ku.edu

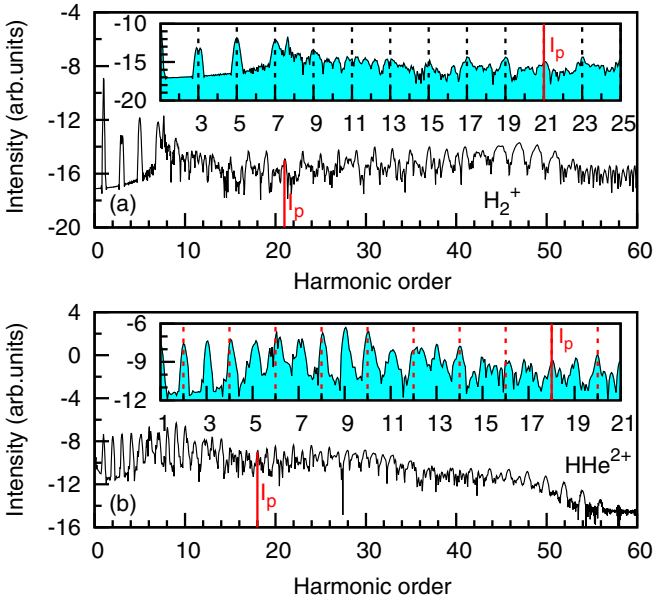

FIG. 1. (a) BTHG of the symmetric H_2^+ molecular ions driven by an 800-nm laser pulse with the intensity $I = 2.0 \times 10^{14}$ W/cm^2. The red vertical solid line indicates the ionization threshold of the $1\sigma_g$ state marked by I_p. (b) BTHG of the asymmetric HHe^{2+} molecular ions by an 800-nm laser pulse with the intensity $I = 1.0 \times 10^{14}$ W/cm^2. The red vertical solid line indicates the ionization threshold of the first excited state 2σ marked by I_p.

the three-dimension Newton's second law of motion in molecular BTHG, we demonstrate how the multiple channels in the molecular BTHG are influenced by the nuclear symmetry. Our results suggest a novel and practical method to realize the enhancement of the BTHG for the vacuum-ultraviolet light sources.

We choose the H_2^+ and HHe^{2+} molecular ions as the symmetric and asymmetric systems, respectively, for the exploration of the dynamical role of the nuclear symmetry on the molecular BTHG in an intense laser field. The H_2^+ and HHe^{2+} molecular ions have been chosen particularly as two-center symmetric and asymmetric molecules due to the following reasons: (i) The H_2^+ and HHe^{2+} possess the symmetric and asymmetric diatomic molecule potentials, which allow us to more easily identify the role of individual quantum channel on molecular BTHG. (ii) The H_2^+ and HHe^{2+} are the simplest one-electron molecular ions, allowing precision numerical treatment by means of the TDGPS method in the prolate spheroidal coordinates [24]. In our calculation, the laser field is written as $E(t) = E_0\cos^2(\pi t/NT)\cos(\omega t)$. Here, E_0 is the electric field amplitude, ω is the frequency, and T is the duration of one optical cycle. The intensity $I = 2.0 \times 10^{14}$ W/cm^2 and $I = 1.0 \times 10^{14}$ W/cm^2 are used for the symmetric H_2^+ and asymmetric HHe^{2+}, respectively. The laser field with the wavelength 800 nm is directed along the molecular axis. The total duration is equal to 20 optical cycles. In Fig. 1(a), we present the BTHG of symmetric H_2^+ molecular ions. The red vertical solid lines indicate the ionization threshold of the initial state marked by I_p. Here I_p is equal to -1.103 a.u. for the $1\sigma_g$ state at the equilibrium internuclear separation of $R = 2$ a.u., which coincides with the 21st harmonic order for the 800-nm laser wavelength. The ionization potential of the $1\sigma_u$ state is -0.668 a.u. The inset shows a more detailed view of the BTHG of H_2^+, and only the odd BTHG spectra are observed. On the other hand, the first resonant peak is located near the seventh harmonic for the 800-nm laser wavelength, which corresponds to the resonance between the initial $1\sigma_g$ state and the first excited state $1\sigma_u$. In Fig. 1(b), we present the BTHG of the HHe^{2+} molecular ions. The red vertical solid lines indicate the ionization threshold of the first excited state 2σ marked by I_p as the initial state with the potential energy -1.031 a.u., which coincides with the 18th harmonic order for the 800-nm laser wavelength. The inset shows a more detailed view of the BTHG of HHe^{2+}. Besides odd harmonic orders in BTHG, even harmonic orders are also observed (see the red dashed lines), which implies that the dynamics of below-threshold harmonic emission have been changed when the nuclear symmetry is broken.

To understand the dynamics of the symmetric and asymmetric molecular BTHG, we present two different dynamical schemes: one for H_2^+ and one for HHe^{2+}, based on an extended classical model that contains the molecular potential. The results are shown in Figs. 2(a) and 2(b), respectively. The orange solid curves indicate the laser field in one optical cycle. In both dynamical schemes, the electron velocity and the electric field force are initially in the opposite directions [27] as the electron moves towards the higher molecular potential. For HHe^{2+} molecular ions, the electronic probability of the first excited state 2σ is mainly on the nuclear H^+, so the electron is driven initially by the intense laser field from the nuclear H^+ nuclear core.

In Fig. 2(a), three distinct channels responsible for the BTHG of H_2^+ are identified. First, in channel 1 ($H_a^+ \rightarrow H_a^+$), the electron is driven back quickly to the parent core on the rising side of the laser field; then in channel 2 ($H_a^+ \rightarrow H_b^+$), the electron is driven from the parent core to the neighbor core; last, in channel 3 ($H_b^+ \rightarrow H_b^+$), the electron is driven back to the initial nuclear core when the laser field reverses the direction. Note that each channel is responsible for the harmonic emission whenever the electron revisits the nuclear core. In Fig. 2(b), five distinct channels responsible for the BTHG of HHe^{2+} are identified. First, in channel 1 ($H^+ \rightarrow H^+$), the electron is driven quickly back to the H^+ nuclear core on the rising side of the laser field; then, in channel 2 ($H^+ \rightarrow He^{2+}$), the electron makes a transition from the H^+ nuclear core to the He^{2+} nuclear core; in channel 3 ($He^{2+} \rightarrow He^{2+}$), after escaping from the He^{2+} nuclear core by tunneling ionization, the electron is driven back by the laser field to the initial nuclear core when the laser field reverses the direction; in channel 4 ($He^{2+} \rightarrow H^+$), the electron makes a transition from the He^{2+} nuclear core to the H^+ nuclear core; last, in channel 5 ($H^+ \rightarrow H^+$), after the electron velocity and the electric field force reach the same direction, the electron is driven away from the H^+ nuclear core, and it returns to the H^+ nuclear core quickly due to the strong binding potential.

It is in general difficult to recognize the origin in BTHG only from the spectral features of H_2^+ and HHe^{2+}. The classical simulation provides complementary information to identify multiple-channel contributions. Although the classical simulation is at best qualitative, its individual channel information provides a clearer physical picture for the

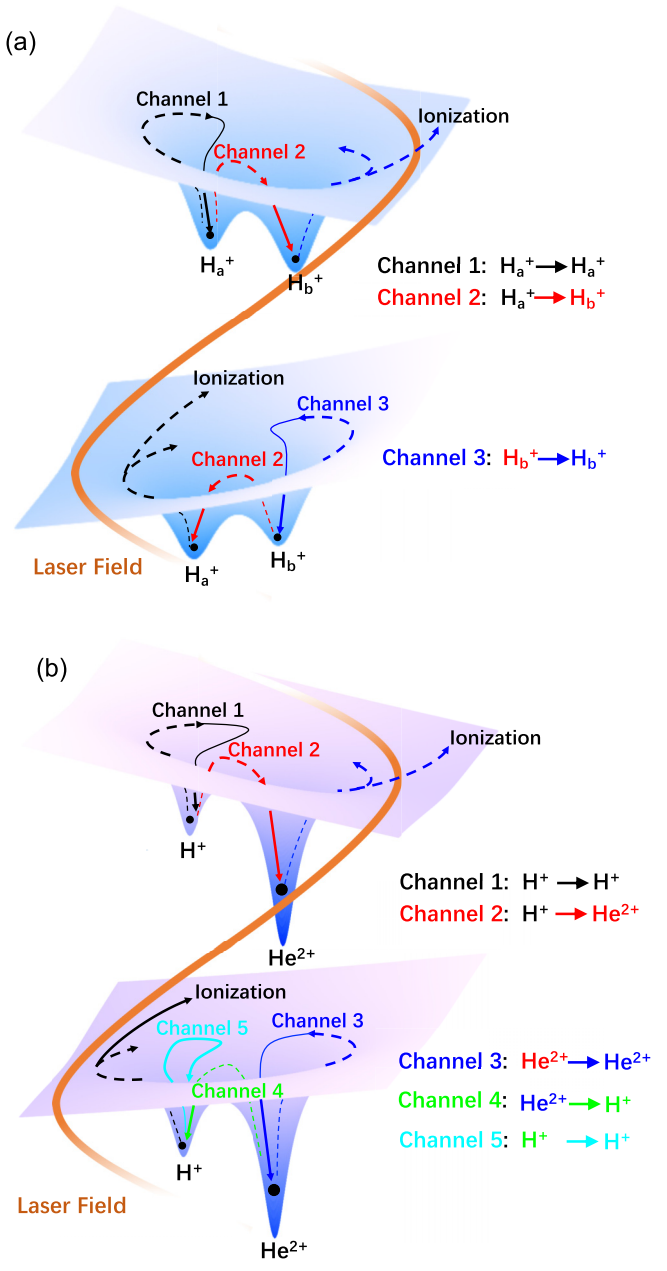

FIG. 2. Dynamical schemes of the BTHG of H_2^+ and HHe^{2+}, respectively. (a) Multiple channels in BTHG for the symmetric H_2^+ molecular ions. (b) Same as (a) for the asymmetric HHe^{2+} molecular ions.

understanding of the BTHG mechanisms. To explore the spectral fine structures of the symmetric and asymmetric molecular BTHG related to the quantum channels, we perform the classical simulations and time-frequency representation (TFR) by the SST transform [26] for H_2^+ and HHe^{2+}, respectively. A detailed classical energy map of multiple channels in the molecular BTHG can be achieved by solving the three-dimensional Newton's equation including the molecular potential. The advantage of the SST transform, as compared to other widely used time-frequency transform, is its capability to generate sharper and clearer time-frequency distributions which allows us to identify the individual contributions below the ionization threshold in time-frequency domain.

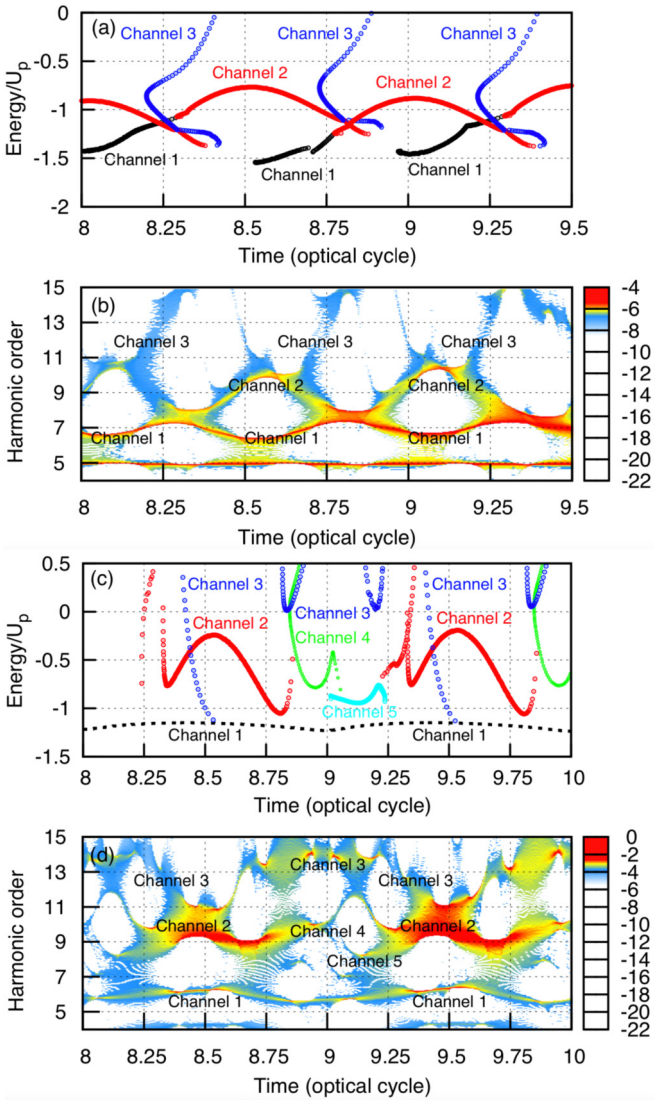

FIG. 3. Classical energy maps and time-frequency representation. (a) Classical return energy as a function of the emission time for the symmetric H_2^+ molecular ions. (b) Time-frequency spectra of H_2^+. (c) Same as (a) for the asymmetric HHe^{2+} molecular ions. (d) Same as (b) for HHe^{2+}. The laser parameters used are the same as those in Fig. 1.

Combining with classical energy maps and time-frequency spectra, we are able to identify the contributions of multiple channels in the BTHG of H_2^+ and HHe^{2+}, respectively.

Figure 3(a) shows the classical return energy as a function of the emission time for the symmetric H_2^+ molecular ions. In our simulations, the initial velocity in the laser polarized direction is zero and it reaches the maximum value at the height of the barrier at the release time; typically, the initial velocities considered are endowed with the transverse momentum [28]. The return energy of electrons includes the kinetic energy and potential energy. Three distinct channels marked by channel 1, channel 2, and channel 3 are again identified, and the intersection of the three channels is found to be located at $-1.2U_p$. Considering the Stark shift of the threshold energy, this energy is in agreement with the seventh harmonic. In Fig. 3(b), the distinct contributions of the multiple channels

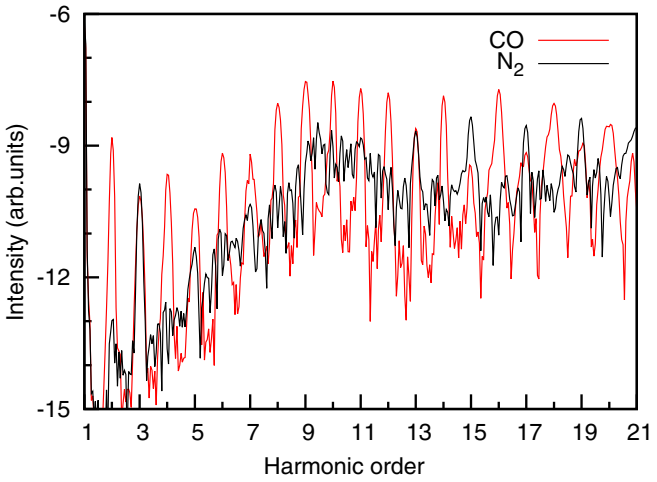

FIG. 4. BTHG of the symmetric N_2 and the asymmetric CO molecules driven by an 800-nm laser pulse with the intensity $I = 1.0 \times 10^{14}$ W/cm^2. The other laser parameters used are the same as those in Fig. 1.

are recognized in the TFR of the BTHG spectra, this result is in good agreement with the classical return energy map shown in Fig. 3(a). In particular, the intersection of three channels is found near the seventh harmonic implying that the multichannel interference is responsible for the enhancement in the BTHG.

Figure 3(c) shows the classical return energy as a function of the emission time for the asymmetric HHe^{2+} molecular ions. Five distinct channels marked by channel 1, channel 2, channel 3, channel 4, and channel 5 are again identified. The energy of channel 2 is $-0.25U_p$ to $-1.1U_p$ in the corresponding harmonics which is located between the 9th harmonic order and the 13th harmonic order. In Fig. 3(d), all quantum channels in the BTHG of HHe^{2+} can be identified in the TFR of the BTHG spectra. We found that channel 2 is dominant and the enhancement may be observed near the ninth harmonic. And the time-frequency spectra of HHe^{2+} are in good agreement with the classical energy map. Moreover, it was found that the contributions from the five different channels are different in the BTHG of HHe^{2+}. Specifically, channels 1 and 5 mainly contribute to the lower-order BTHG, while channels 2 and 4 can be related to the electron transitions between the nuclear cores H^+ and He^{2+} and contribute to the near- and below-threshold harmonic emission. Finally, channel 3 mainly contributes to the higher-order harmonic emissions. The most significant finding is that a dominant contribution comes from channel 2 which is associated with the electron transition from the nuclear cores H^+ to He^{2+}. As a result, the electron transition from the light nuclear core to the heavy nuclear core features mostly constructive interference, due to a strong permanent dipole, which is responsible for the strong emission of the asymmetric molecular BTHG. These findings point out an important fact that the asymmetric molecular systems are amenable to the enhancement of the BTHG.

To further confirm our findings, we present all-electron TDDFT calculations of the BTHG of the symmetric N_2 and asymmetric CO molecules in intense laser fields as shown in Fig. 4. N_2 and CO are isoelectronic molecules, both having 14 electrons and triple bonds. The highest occupied molecular orbital ionization potentials for N_2 ($3\sigma_g$) and CO (5σ) are very close to each other. That is why N_2 and CO have similar ionization behaviors in the laser field with the same wavelength and intensity. For both N_2 and CO, the laser field is assumed to be parallel to the internuclear axis, and the internuclear distances for the CO ($R = 2.132$ a.u.) and N_2 ($R = 2.072$ a.u.) molecules are fixed at their individual equilibrium distances. Results for the wavelength of 800 nm with the laser intensity $I = 1.0 \times 10^{14}$ W/cm^2, 20-optical-cycle laser pulse are shown for CO and N_2, respectively. The other laser parameters used are the same as those in Fig. 1. In Fig. 4, one can see that the BTHG is more efficient in CO than in N_2. We find that the whole BTHG of CO is enhanced by two orders of magnitude by comparing with the case of N_2. As discussed above, there is a new dynamic besides resonance effects for the asymmetric molecules that can lead to the enhancement of the whole BTHG, namely, the nuclear symmetry effect. The reason for it is that the number of dominant emissions per optical cycle is now limited to the channel 2 as shown in Figs. 3(c) and 3(d) and this particular emission is largely enhanced. Most importantly for the CO molecule, a distinct feature of the BTHG possibly characteristic of all asymmetric diatomic systems is observed as shown in Fig. 4.

In conclusion, we have investigated the role of the nuclear symmetry on the molecular harmonic generation below the ionization threshold in an intense laser field by means of accurately solving the TDSE and TDDFT. Combining with classical energy maps and time-frequency spectra, we have identified the contributions of multiple channels in the BTHG of H_2^+ and HHe^{2+}, respectively. It was found that three distinct channels are responsible for the BTHG of H_2^+, while five distinct channels are responsible for the BTHG of HHe^{2+}. These channels are related to the electron driven by the laser field at specific times of laser pulse from one nuclear core back to either a neighboring ion or the parent ion itself. In particular, for the asymmetric nature of molecules, the electronic transition from the light nuclear core to the heavy nuclear core features mostly constructive interference leading to the dramatic enhancement of the BTHG. The latter observation shows that the heavy nuclear core plays an important role in the electron-nuclear coupled dynamics of the asymmetric molecular system. In addition, we have presented a comparison of the BTHG of the symmetric N_2 and asymmetric CO molecules in intense laser fields. The result shows a large enhancement of the BTHG for the CO molecule over that of the N_2 molecule. Our findings provide a deep understanding of molecular BTHG dynamics and spectroscopy and shed light on a practical method for the enhancement of the BTHG for the vacuum-ultraviolet light sources.

This work was supported by the National Natural Science Foundation of China (Grants No. 11674268, No. 11674209, No. 11774215, No. 11764038, and No. 91850209) and Department of Education of Guangdong Province (Grant No. 2018KCXTD011), China. We also would like to acknowledge the partial support of the Ministry of Science and Technology (MOST), Taiwan, and the National Taiwan University (Grants No. 108L893201 and No. 108L104048). The authors would also like to thank Dr. Tak-San Ho (Princeton University) for helpful discussions.

[1] F. Krausz and M. Ivanov, Rev. Mod. Phys. **81**, 163 (2009).
[2] Y. Mairesse, A. de Bohan, L. J. Frasinski, H. Merdji, L. C. Dinu, P. Monchicourt, P. Breger, M. Kovačev, R. Taïeb, B. Carré *et al.*, Science **302**, 1540 (2003).
[3] M. Chini, K. Zhao, and Z. H. Chang, Nat. Photonics **8**, 178 (2014).
[4] P. B. Corkum, Phys. Rev. Lett. **71**, 1994 (1993).
[5] K. C. Kulander, K. J. Schafer, and J. L. Krause, in *Proceedings of the Workshop on Super-Intense Laser Atom Physics (SILAP) III*, NATO ASI Series Vol. 316, edited by P. Piraux (Plenum Press, New York, 1993), p. 95.
[6] D. C. Yost *et al.*, Nat. Phys. **5**, 815 (2009).
[7] J. Henkel, T. Witting, D. Fabris, M. Lein, P. L. Knight, J. W. G. Tisch, and J. P. Marangos, Phys. Rev. A **87**, 043818 (2013).
[8] E. P. Power *et al.*, Nat. Photonics **4**, 352 (2010).
[9] M. Chini *et al.*, Nat. Photonics **8**, 437 (2014).
[10] C. C. Chirilă, I. Dreissigacker, E. V. van der Zwan, and M. Lein, Phys. Rev. A **81**, 033412 (2010).
[11] P. Antoine, B. Piraux, and A. Maquet, Phys. Rev. A **51**, R1750 (1995).
[12] P. C. Li, Y. L. Sheu, C. Laughlin, and Shih-I Chu, Phys. Rev. A **90**, 041401(R) (2014).
[13] J. Itatani *et al.*, Nature (London) **432**, 867 (2004).
[14] T. Kanai, S. Minemoto, and H. Sakai, Nature (London) **435**, 470 (2005).
[15] R. Velotta, N. Hay, M. B. Mason, M. Castillejo, and J. P. Marangos, Phys. Rev. Lett. **87**, 183901 (2001).
[16] M. Lein, N. Hay, R. Velotta, J. P. Marangos, and P. L. Knight, Phys. Rev. Lett. **88**, 183903 (2002).
[17] H. Soifer, P. Botheron, D. Shafir, A. Diner, O. Raz, B. D. Bruner, Y. Mairesse, B. Pons, and N. Dudovich, Phys. Rev. Lett. **105**, 143904 (2010).
[18] K. Nasiri Avanaki, D. A. Telnov, and Shih-I Chu, Phys. Rev. A **90**, 033425 (2014).
[19] J. Heslar and Shih-I Chu, Sci. Rep. **6**, 37774 (2016).
[20] D. A. Telnov and Shih-I Chu, Phys. Rev. A **76**, 043412 (2007).
[21] E. Runge and E. K. U. Gross, Phys. Rev. Lett. **52**, 997 (1984).
[22] E. K. U. Gross and W. Kohn, Phys. Rev. Lett. **55**, 2850 (1985).
[23] X. Chu and Shih-I Chu, Phys. Rev. A **63**, 023411 (2001).
[24] D. A. Telnov and Shih-I Chu, Phys. Rev. A **80**, 043412 (2009).
[25] X. M. Tong and Shih-I Chu, Chem. Phys. **217**, 119 (1997).
[26] H. T. Wu, Y. H. Chan, Y. T. Lin, and Y. H. Yeh, Appl. Comput. Harmon. Anal. **36**, 354 (2014).
[27] P. C. Li, Y. L. Sheu, C. Laughlin, and S. I. Chu, Nat. Commun. **6**, 7178 (2015).
[28] See Supplemental Material at http://link.aps.org/supplemental/10.1103/PhysRevA.101.011401 for the choice of initial velocity.